Magnetic structure factor and pair correlation function for a semiconductor quantum wire

2007 J. Phys.: Condens. Matter 19 306201

(http://iopscience.iop.org/0953-8984/19/30/306201)

IOP PUBLISHING JOURNAL OF PHYSICS: CONDENSED MATTER

J. Phys.: Condens. Matter **19** (2007) 306201 (11pp) doi:10.1088/0953-8984/19/30/306201

Magnetic structure factor and pair correlation function for a semiconductor quantum wire

S S Z Ashraf[1], A C Sharma[2] and K N Vyas[2]

[1] Physics Department, Shibli National PG College, Azamgarh-276001, UP, India
[2] Physics Department, Faculty of Science, The MS University of Baroda, Vadodara-390 002, India

Received 10 March 2007, in final form 21 May 2007
Published 3 July 2007
Online at stacks.iop.org/JPhysCM/19/306201

Abstract

In this paper we report the spin correlation and its effects on the many-body properties of a quantum wire whose width is given practical consideration. The single-pole approximation, which is of much relevance in studying the many-body properties of an interacting one-dimensional electron gas (1DEG) because of the severe constraints imposed on the phase space of plasma–hole excitations, has been used to obtain analytical results. The local-field corrections are incorporated within the Hubbard approximation (HA). We find the results obtained for low electron densities under the single-pole approximation on the paramagnon dispersion relation, magnetic structure factor and the symmetric and anti-symmetric pair correlation function to be in good quantitative agreement with those obtained under heavily computational self-consistent field calculations. Unlike prior reported work on the magnetic structure factor and pair correlation function, our calculation is applicable to quantum wires of width less than 10 nm, where interesting quantum size effects are observed.

1. Introduction

The spin of the electron in low-dimensional systems has been the subject of investigation in an increasing number of experimental and theoretical studies over the past few years. Magnetic phenomena apart, it has been reported that spin can also play a nontrivial role even in nonmagnetic phenomena [1]. Conductance measurements on ultra-low-disorder quantum wires support a spin polarization at zero magnetic field. Spin–spin interactions are suggested to be responsible for the so-called experimentally established 0.7 structures [2]. It has recently been shown by thermodynamic measurements that the Pauli spin susceptibility of a strongly correlated two-dimensional electron liquid in silicon grows critically at low electron densities, which is suggestive of the existence of a phase transition [3]. A separate subject of spintronics, which is a neologism for spin-based electronics (also known as magnetoelectronics) which exploits the use of the quantum propensity of electrons to spin as well as making use of their charge state, has already made significant technological progress in recent times [4]. The

ability to control electron spins in molecules leads to molecular spintronics, which is seen as an alternative to silicon in complementary metal oxide semiconductors [5]. It is envisioned that a complete understanding of the spin polarization will have immediate applications to one-dimensional (1D) transport in mesoscopic devices and will also have implications in the area of spintronics.

In 1D and quasi-1D, system interactions become increasingly noticeable at low densities. The enhanced interactions (in principle—because of the occurrence of Peierls divergence in the particle–hole bubble and charge spin separation) invalidate the celebrated Fermi liquid model which describes the low-energy dynamics of interacting normal solid-state bulk systems. As a consequence of the electron–electron interactions, a correlated 1D system is expected to exhibit Tomonaga–Luttinger (TL) behaviour [6]. However, the ordinary Fermi liquid theory has been reported to be valid in the presence of disorder, which always exists, in a real 1D electron gas system, also termed a quantum wire (QW) at finite temperature [7]. Also, the TL model still does not account for many of the peculiarities of the 1D system. For example, the TL model is unequipped to explain the occurrence of the much discussed 0.7 structure, i.e. $0.7(2e^2/h)$ conductance plateaus, at zero temperature [8].

The paramagnetic ground state of the electron gas at high densities spontaneously switches to a spin-polarized ferromagnetic state at low densities due to the enhanced interactions which induce correlation between the electrons. Spin fluctuations can be treated by introducing the local field correction (LFC) for the spin susceptibility, which results in a Stoner-like enhancement factor [9]. The short-range spin exchange and correlation effects in a QW have been studied under various schemes such as Singwi–Tosi–Land–Sjölander (STLS) and Singwi–Sjölander–Tosi–Land (SSTL) via an LFC in the spin density response function [10–13]. An expression for the frequency- and wavevector-dependent paramagnetic susceptibility of a three-dimensional electron gas at metallic densities was derived within the random phase approximation (RPA) by Lobo, Singwi and Tosi (LST) [14]. The LST approach uses the concept of the LFC for the spin susceptibility for the electron gas with long-range Coulomb interaction. The LFC takes into account the deviations from the RPA due to the effects of exchange and correlation. The influence of exchange correlation in a quantum wire has been re-emphasized courtesy of a recent experiment on the measurement of 1D plasmons in an atom wire array on the Si(557)-Au surface by inelastic scattering of a highly collimated slow electron beam. Though the experiment has been conducted on a high-density free-electron gas, a substantial influence of electron correlation due to strong 1D confinement has still been detected [15]. Apart from the self-consistent calculations, there have been studies of the 1DEG using diffusion Monte Carlo simulations to estimate the ground-state properties by taking into consideration the effects of exchange and correlation [16].

Recently, the spin correlation effects in a QW have been investigated in the STLS and compared with the SSTL approach [13]. A few of the physical quantities have also been calculated considering the LFC within the HA for spin correlations, and the results are found overall to be in good agreement with those of SSTL and STLS but particularly in closer agreement with that obtained in the STLS method. The various competing schemes like the Hubbard approximation, STLS and SSTL, as mentioned above, estimate the exchange and correlation effects. These have been formulated to improve upon the limitations of the other, but in turn their own loopholes and shortcomings creep in. For example the STLS, although a big improvement over the RPA for considering short-range correlation, gives a correct pair correlation function but fails to satisfy the compressibility sum rule, whereas the SSTL approach, which satisfies the compressibility rule better than the STLS method, yields a negative value of the pair correlation function [13]. It has been observed that the replacement of one with other brings in only a marginal change in the calculated physical properties of the QW [12, 13].

One of the two concerning aspects of the prior reported studies on the ground-state properties of the QW is the consideration of width of the generic semiconductor QW. The characteristic quantum features of a QW, such as a significant change in the fundamental band gap and a reduction in the dielectric constant determining the binding and exchange energies, emerges when the QW is restricted to at most the single-nanometre (nm) digit range [17, 18]. The bulk properties of semiconductor QWs are not affected down to the smallest commercial submicron devices [19, 20]. Also, for the room-temperature operation of a quantum device the various calculated length-scales fall into this single-nanometre limit [21]. Secondly, a great deal of interest in the 1D structures has been due to the fact that these structures have offered a realistic platform for testing various theoretical predictions like TL behaviour, Peierls distortion, Anderson localization etc. But the tests have traditionally utilized 3D crystals containing chain structures, such as chains of transition-metal ions spaced by counter-ions or conjugated polymer chains. However, in the recent past there have been attempts to go beyond these limited classes of compounds and tailor 1D chain structures at surfaces in order to customize their electronic structure, such as controlling the chain–chain interaction, altering the band filling and secluding a Peierls distortion [21]. However theoretical investigations on correlation effects in a QW have been performed on 1D systems having widths of more than 10 nm. Therefore there appears to be a need to perform calculations on the spin correlation effects in a QW for a width spanning less than 10 nm.

The single-pole approximation (SPA) is of the utmost significance in studying the properties of quantum wire systems because of the severe restrictions in the phase space of the particle–hole excitations, as has been argued convincingly in the recent past [22]. The SPA is referred to as a plasma pole approximation (PPA) in the calculation of ground-state properties involving the density response function. The calculated electron self-energy due to Coulomb interaction and the hot electron energy relaxation rate due to longitudinal optic (LO) phonon emission in GaAs quantum wires using PPA are almost found to be identical with more complete many-body calculations [22]. The PPA is a very good approximation to the RPA in QW systems, as the plasmon excitations dominate the single-particle excitations. The TL liquid model also proposes that the true coherent excitations of the ideal 1D system are the collective charge density excitations which are of bosonic character, and the single-particle excitations are nonexistent. Also, the dispersion of the TL bosons to third order in q is exactly similar as for the plasmons calculated within the RPA. The plasmon modes in a QW exist for all wavevectors which are unlike higher dimensions [7]. Earlier, the PPA was used extensively in the calculation of electron self-energies of three- and two-dimensional systems, and the results obtained have been found to be in good semi-quantitative agreement with those of more complete RPA and experimental data [22].

In light of these arguments and as a sequel to our reported study on the spin-independent many-body aspects of a QW [23], in this paper we report the calculated spin-correlated ground-state properties of a QW, where the LFC are incorporated within the HA and the width of the QW is given practical consideration. The calculations are made within the SPA as well as beyond the SPA. The paper has been organized as follows: section 2 describes the model and theory used in this work; section 3 contains the results and discussion; and finally section 4 concludes the work.

2. Model and theory

Our study is modelled on a GaAs-QW which is parameterized in terms of the effective mass $m^* = 0.068m_e$ and the background dielectric constant $\varepsilon_b = 12.5$. The construction of the QW is defined by δ-function-type confinement along the z-axis and an infinite-potential-well-type

confinement along the y-axis, with the electrons free to move along the x-axis. The electron wavefunction is assumed to vanish at boundaries of the wire across the y-axis, at $y = \pm a/2$, where a is the width of a QW. The band for motion along the x-axis is assumed to be parabolic; $\xi_k = \frac{\hbar^2 k^2}{2m^*} - \mu$, where m^* is the effective electron band mass and μ is the chemical potential. This is a reasonable assumption for a QW where the electron density is low ($\sim 10^6$ cm^{-1}), occupying only the lowest (ground) subband.

The static structure factor and static magnetic structure factor, respectively, can be expressed as [13, 24]

$$S(q) = \frac{-1}{n\pi} \int_0^\infty \mathrm{d}\omega \, \mathrm{Im}(\chi^d(q,\omega)) \tag{1}$$

$$\hat{S}(q) = \frac{1}{n\pi g^2 \mu_\mathrm{B}^2} \int_0^\infty \mathrm{d}\omega \, \mathrm{Im}(\chi^s(q,\omega)), \tag{2}$$

where n is the 1D density related to the Fermi wavevector, k_F, by the relation $n = 2k_\mathrm{F}/\pi$. The zero-temperature dynamic density–density response, $\chi^d(q,\omega)$, and the spin-density response function, $\chi^s(q,\omega)$, respectively, are defined as [13]

$$\chi^d(q,\omega) = \frac{\chi_0(q,\omega)}{1 - V_\mathrm{s}^\mathrm{eff}(q)\chi_0(q,\omega)} \tag{3}$$

$$\chi^s(q,\omega) = -g^2\mu_\mathrm{B}^2 \frac{\chi_0(q,\omega)}{1 - V_\mathrm{a}^\mathrm{eff}(q)\chi_0(q,\omega)}. \tag{4}$$

$\chi_0(q,\omega)$ is the zero-temperature irreducible polarizability function, $g\mu_\mathrm{B}$ is the magnetic moment of an electron in which g is the Lande factor, and μ_B is the Bohr magnetron. The real and imaginary parts of $\chi_0(q,\omega)$ are defined and evaluated for a QW in [23]. $V_\mathrm{s}^\mathrm{eff}(q)$ and $V_\mathrm{a}^\mathrm{eff}(q)$ are the symmetric and antisymmetric spin effective potentials, respectively, defined as follows:

$$V_\mathrm{s}^\mathrm{eff}(q) = V^0(q)[1 - G(q)] \tag{5}$$

$$V_\mathrm{a}^\mathrm{eff}(q) = V^0(q)\, G^s(q), \tag{6}$$

where $V^0(q)$ is the Fourier transform of the bare Coulomb potential for a QW. Most of the previously conducted studies have taken the bare Coulomb potential described by the harmonic confinement potential [10–13],

$$V^0(q) = (e^2/\varepsilon_0)\mathrm{e}^x k_0(x), \tag{7}$$

with $x = (qb/2)^2$, where b is the lateral width of the QW, determined by the confining oscillator frequency, and $k_0(x)$ is a modified Bessel's function of the second kind. However, this potential does not give a true description of the bare Coulomb potential for a QW of smaller width ($a < 5$ nm). Therefore, as has been discussed earlier, for practical considerations we undertake a more suitable form of $V^0(q)$ that gives a better description of the bare Coulomb potential for a QW and remains valid at all values of q and a. The $V^0(q)$ that we adopt is defined by [23]

$$V^0(q) = \frac{2e^2}{\varepsilon_0} \int_0^\infty \mathrm{d}t \frac{H(u)}{\sqrt{t^2 + q^2}}, \tag{8}$$

with

$$H(u) = \left(\frac{u}{w} + \frac{2}{u}\right) - \frac{32\pi^4}{(wu)^2}(1 - \mathrm{e}^{-u}), \tag{9}$$

where $u = a\sqrt{t^2 + q^2}$ and $w = u^2 + 4\pi^2$. The LFC for density fluctuation, $G(q)$, and for spin fluctuation, $G^s(q)$, for a QW can be given in the HA by [23, 13]

$$G(q) = \frac{1}{2}\frac{V^0\left(\sqrt{q^2+k_F^2}\right)}{V^0(q)} \tag{10}$$

$$G^s(q) = -\frac{1}{2}\frac{V^0\left(\sqrt{q^2+k_F^2}\right)}{V^0(q)}. \tag{11}$$

The HA does away with the heavy computational work required in other self-consistent calculation schemes, such as SSTL and STLS, and it makes the calculation of the ground-state properties relatively simple. Further, firstly, as the single-particle excitations are nonexistent in 1D, courtesy of the TL model, and the collective excitations that emerge in this model are bosons, so it looks academically more plausible and consistent to invoke the SPA in studying the many-body properties of a 1D interacting electron gas. The utilization of SPA puts the formalism on the same footing as that of the TL framework. The SSTL and STLS (albeit more accurate than Hubbard) are still based on the Fermi liquid picture, and this aspect calls for an explanation, as the standard theoretical model has been the TL model. Secondly, the calculation of many-body properties in the SPA helps to obtain a few analytical results, as have been duly reported before [23]. Under the SPA, equation (2) reduces to

$$\hat{S}(q) = \frac{1}{n\pi}\int_0^\infty d\omega \frac{\chi_{02}}{(1-\frac{\omega_s^2}{\omega^2})^2 + (V_a^{\rm eff}\chi_{02})^2}. \tag{12}$$

ω_s is the frequency of intra-subband collective spin density excitations, termed paramagnons, defined by the poles of the spin correlation response function, i.e. $1/\chi^s(q,\omega) = 0$. The dispersion of the collective modes is given by the simple analytical result [25]. The expression for ω_s can be generalized for any other method like SSTL and STLS by incorporating the LFC. In the HA, ω_s is given by

$$\frac{\omega_s}{\varepsilon_F} \equiv y_0 = \left[\frac{A^s(q)\omega_+^2(q) - \omega_-^2(q)}{A_s(q)-1}\right]^{1/2}, \tag{13}$$

where $A^s(q) = e^{q\pi/mV_a^{\rm eff}(q)}$, and $\omega_\pm = |E_q \pm q v_F|$ defines the limits of the single-particle excitations. $\varepsilon_F = \hbar^2k_F^2/2m^*$ is the free-electron Fermi energy and $E_q = \hbar^2q^2/2m^*$. Equation (13) can also be cast as

$$y_0^2 = \left(\frac{8z^3}{A^s(q)-1}\right) + (z^2+2z)^2, \tag{14}$$

where we define $z = q/k_F$. A central role is played by the electron pair correlation function. Accurate knowledge of this function is crucial for applications of density functional theory in various schemes that have been proposed to transcend the local density approximation in the construction of exchange and correlation energy functionals [26]. The Fourier transform of the static structure factor and static magnetic structure factor give the nonmagnetic and magnetic pair correlation functions, respectively, which take the form below:

$$g(r) = 1 + \tfrac{1}{2}\int_0^\infty dq\ \cos(qr)[S(q)-1] \tag{15}$$

$$\hat{g}(r) = \tfrac{1}{2}\int_0^\infty dq\ \cos(qr)[\hat{S}(q)-1]. \tag{16}$$

The parallel spin pair correlation function, $g\uparrow\uparrow(r)$, and the anti-parallel spin pair correlation function, $g\uparrow\downarrow(r)$, may be written in terms of equations (15) and (16), respectively, as;

$$g\uparrow\uparrow(r) = g(r) + \hat{g}(r) \tag{17}$$

$$g\uparrow\downarrow(r) = g(r) - \hat{g}(r). \tag{18}$$

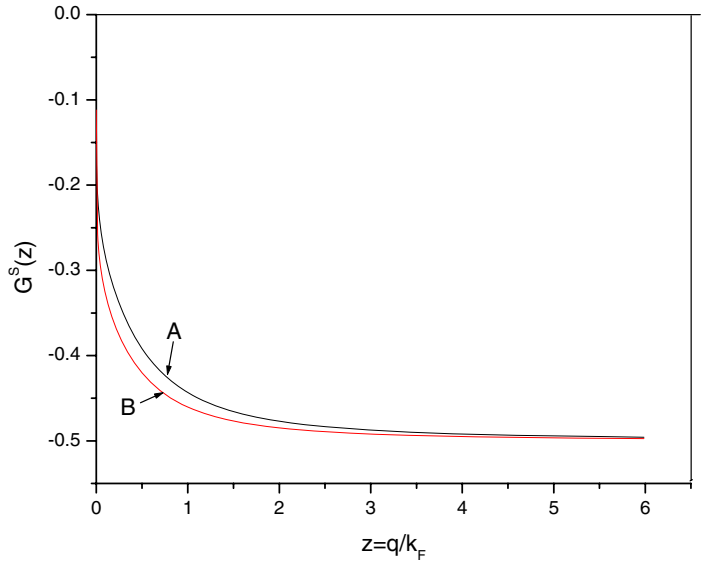

Figure 1. Local-field correction, $G^{s}(z)$, plotted as a function of z. The figure depicts curve A for $r_s = 1$ and $a = 5$ nm, and curve B for $r_s = 4$ and $a = 5$ nm.

(This figure is in colour only in the electronic version)

3. Results and discussion

Figure 1 displays the $G^{s}(z)$ within HA for two different values of $r_s = 1/(2na_B)$, where $a_B = \varepsilon\hbar^2/e^2m^*$ is the Bohr radius and e is the electronic charge. A small ratio of the Coulomb energy, E_c and ε_F, i.e. $E_c/\varepsilon_F \ll 1$, is suggestive of high electron densities and weak electron–electron interactions, and conventional Fermi liquid behaviour is applicable. On the other hand, $E_c/\varepsilon_F \gg 1$ means that very low electron densities and strong electron–electron interactions are rampant, which results in a highly correlated electron liquid, where the formation of a Wigner crystal is expected. The LFC incorporate the effects of correlation and thereby plays an important role in determining physical quantities that involve many-body interactions. They also influence the fulfilment of sum-rules. The incorporation of LFC in the scheme extends the range of q-values over which sum-rules can be satisfied and that the range is determined by the value of $G^{s}(z)$. We had checked the compliance of other sum-rules too and found that the formalism adopted by us conforms to them for $q \to 0$ [23, 27]. From the plot of $G^{s}(z)$, from equation (11) in figure 1 for two values of k_F ($= 0.8074 \times 10^6$ and $0.201\,85 \times 10^6$) cm^{-1} (which correspond to $r_s = 1$ and 4, respectively) and the width of the QW spans 5 nm, we find that the correlation between the electrons increases with decreasing density, that is, increasing r_s. The paramagnon dispersion, ω_s, versus $z = q/k_F$ at $r_s = 2$ is shown in figure 2. The curve exhibits the same linear behaviour as has been found in computations using the SSTL and STLS approaches for small values of z [13].

The $\hat{S}(z)$ evaluated in the HA that has been used in our calculation is very similar to that obtained from the SSTL [12] and STLS [13] schemes of computation. All three evaluations are similar to the Hatree–Fock result for a free-electron gas at small values of r_s. However, no analytical result is possible for $\hat{S}(z)$ in the STLS and SSTL schemes of incorporating the LFC. The advantage of our approach of calculating $\hat{S}(z)$ using HA over the SSTL and SSTL method is that an analytical result can be obtained for the magnetic structure factor by the use of the

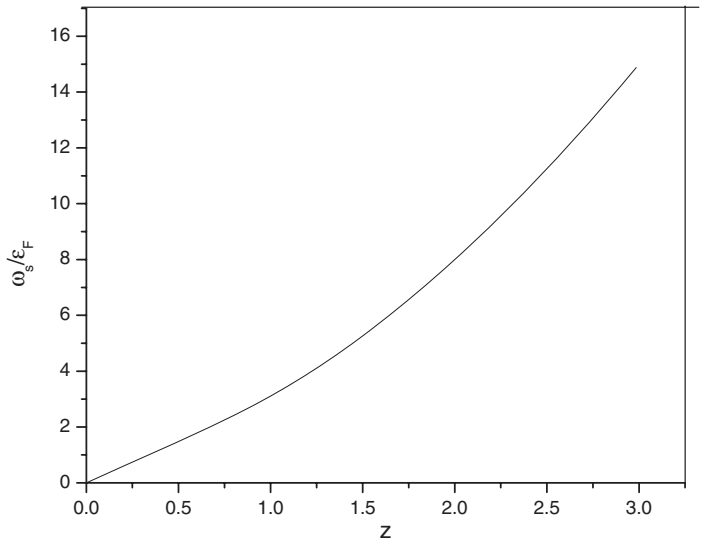

Figure 2. Paramagnon dispersion, $\omega_S(z)/\varepsilon_F(z)$ is plotted as a function of z for $r_s = 2$.

SPA. Our calculated analytical results on $\hat{S}(z)$ using the SPA are given by,

$$\hat{S}(z) = \frac{2z^2}{t^2} + \frac{by_0^2(2+t)}{4rt^3}\log\left(\frac{(ty_2^2+y_0^2-y_2r)(ty_1^2+y_0^2+y_1r)}{(ty_1^2+y_0^2-y_1r)(ty_2^2+y_0^2+y_2r)}\right) + \frac{by_0^2(2-t)}{2\sqrt{\Delta}t^3}\left\{\tan^{-1}\left(\frac{2ty_2+r}{\sqrt{\Delta}}\right)+\tan^{-1}\left(\frac{2ty_2-r}{\sqrt{\Delta}}\right) - \tan^{-1}\left(\frac{2ty_1-r}{\sqrt{\Delta}}\right)-\tan^{-1}\left(\frac{2ty_1+r}{\sqrt{\Delta}}\right)\right\}, \tag{19}$$

where

$$b = \frac{m^* V_a^{\text{eff}}}{zk_F\hbar^2}, \qquad y_2 = z(z+2), \qquad y_1 = z(z-2), \qquad t = \sqrt{1+b^2},$$

$$r = \sqrt{2y_0(1+t)}, \qquad \Delta = \sqrt{4y_0^2t - r^2}.$$

As for the case of $S(z)$ calculated within the HA using the PPA, the $\hat{S}(z)$ worked out under HA with the use of the SPA describes very well the behaviour of numerically computed results on $\hat{S}(z)$ from equation (2) within the HA, for lower values of z.

Figures 3(a) and (b) depict the magnetic structure factor for varying densities ($r_s = 0.5, 1, 2$) and wire widths ($a = 20$, 9, 5 nm), respectively, evaluated using equations (2) and (19). The plotted $\hat{S}(z)$ versus z curves ((A) and (D)) in figure 3(a) for $r_s = 0.5$ develop a peak at $z = 2$. This trend is also seen in both the self-consistent calculations of SSTL and STLS, for values of r_s up to $r_s = 1.5$, beyond which it becomes exceedingly difficult to obtain self-consistent solutions for a magnetic structure factor, although it is possible in the case of a nonmagnetic structure factor. The peaks observed have been argued to be suggestive of paramagnetic instability [11, 12]. A recent self-consistent field calculation on the exchange coupling in mesoscopic rings using the LST formalism also shows a peak in the magnetic structure factor [28]. The magnetic structure factor evaluated in the HA formalism does not impose an upper limit on the values of r_s to obtain a solution, however it can be observed from

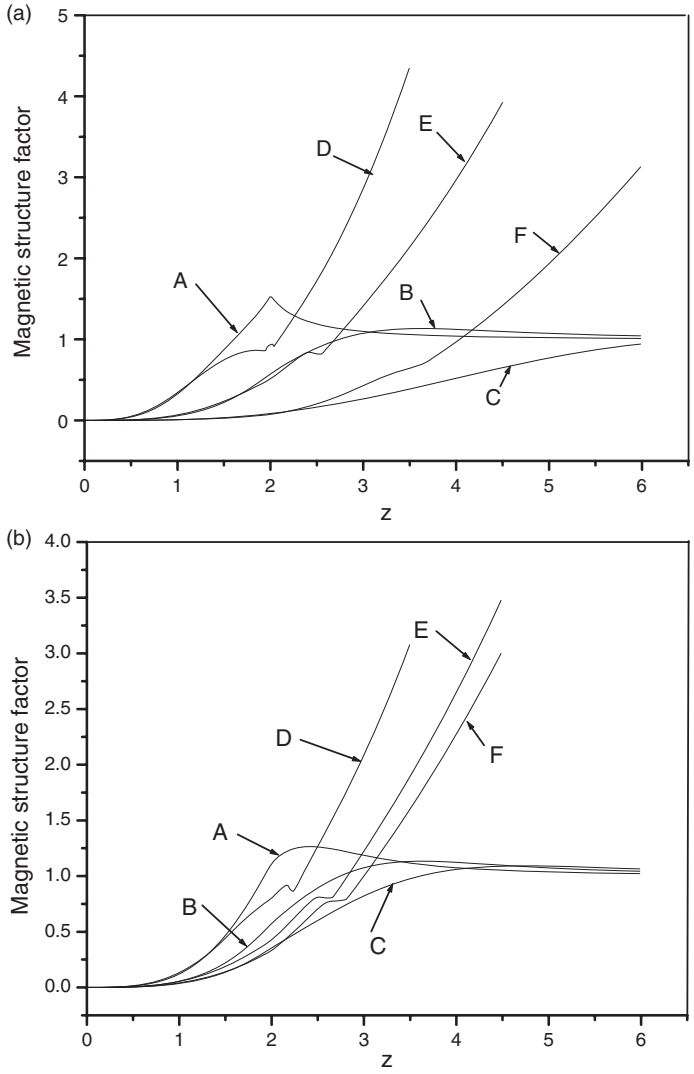

Figure 3. (a) Analytical magnetic structure factor within the SPA (curves D, E and F) along with the numerically computed $\hat{S}(z)$ from equation (2) (curves A, B and C) are plotted for QW constant width; $a = 9$ nm and varying densities r_s. Curves A and D are plotted for $r_s = 0.5$, curves B and E are plotted for $r_s = 1$, and curves C and F are plotted for $r_s = 2$. (b) Analytical magnetic structure factor in the SPA (curves D, E and F) along with the numerically computed $\hat{S}(z)$ from equation (2) (curves A, B and C) are plotted for constant density $r_s = 1$ and varying QW width a. Curves A and D are plotted for $a = 20$ nm, curves B and E are for plotted for $a = 9$ nm, and curves C and F are plotted for $a = 5$ nm.

curves B and E, C and F in figure 3(a) that the peak smooths out for increasing values of r_s. The peak not only depends on density but it is very much influenced by the width of the QW. The same can be figured out from figure 3(b), where it can be noticed that the broad peak observed for $a = 20$ nm in the case of numerical $\hat{S}(z)$ (curve A) and a relatively sharp peak in the SPA (curve D) tends to flatten for decreasing values of the parameter a. At relatively high density, $r_s = 0.8$, and thick wire diameter ($a/a_B = 3.1$), it has been shown that the dispersion of the

RPA plasmon and the dispersion calculation within the TL model are essentially identical for small momentum transfers $z \leqslant 0.2$ [29]. Therefore, the analytical result for $\hat{S}(z)$ obtained in the SPA is of significance, as it exactly reproduces the result of the more exhaustive HA $\hat{S}(z)$ for small z values, even for much smaller wire widths and larger r_s than in the above-quoted paper. It is well established that the SPA complies with the f-sum rule and the static Kramers–Kronig relation [15, 17]. In fact, the HA $\hat{S}(z)$ within the SPA agrees with the HA $\hat{S}(z)$ beyond the SPA for greater values of z. The SPA magnetic analytical structure factor that incorporates LFC within the HA also exhibits a peak at $q = 2k_F$, as obtained from the more exhaustive numerical structure factor shown in figure 3(a). However, the behaviour of the analytical $\hat{S}(z)$ is a little different from the analytical $S(z)$, which is akin to the case of numerical $\hat{S}(z)$ and $S(z)$. The $\hat{S}(z)$ shows a small peak at some value of z, depending on the value of r_s, and then increases with increasing values of z, unlike the $S(z)$, which continuously increases for all values of z. The monotonously increasing analytical $\hat{S}(z)$ for increasing z values seems to be unphysical, but the exactness of the result for lower z values is sufficient to speak of its utility to a point. The STLS calculation is also reported to exhibit a peak, but the peak vanishes for densities $r_s > 1.8$. The STLS approach employs the bare Coulomb potential and the SSTL computation is performed using a screened Coulomb potential. In our approach too, the peak begins to diminish for decreasing values of electron densities and ultimately is not seen for higher values of r_s.

The graphs of spin symmetric pair correlation function, $g\uparrow\uparrow(r)$, and spin anti-symmetric pair correlation function, $g\downarrow\uparrow(r)$, calculated within the Hubbard approximation along with the $g\uparrow\uparrow(r)$ and $g\downarrow\uparrow(r)$ obtained in the SPA is displayed in figures 4(a) and (b), respectively, for two values of r_s (1 and 0.323) or k_F (0.8074×10^6 and 2.5×10^6) cm^{-1}. The values of $g\downarrow\uparrow(r)$ depicted in figure 4(b), for the correlation between anti-parallel spins, is governed only by the Coulombic repulsion of the electrons, whereas statistics play a role in the correlation of parallel spin electrons—$g\uparrow\uparrow(r)$. As reported earlier, the $g\uparrow\uparrow(r)$ remains independent of r_s for higher values of $r_s (r_s > 0.323)$. Also, the fact that values of $g\uparrow\uparrow(r)$ at zero separation increase with increasing r_s, as has been reported in [12, 13], is also clearly demonstrated in our calculation within the HA for both the cases of the SPA and without the SPA. It is found that the curve of $g\uparrow\uparrow(r)$ under the SPA approaches that of $g\uparrow\uparrow(r)$ computed without the SPA, for higher values of r_s ($r_s > 1$). Our computed $g\uparrow\uparrow(r)$ yields negative values for lower values of separation, when $r_s < 0.323$ or ($k_F > 2.5 \times 10^6$ cm^{-1}) at $a = 7$ nm. The calculation using STLS is not free from this shortcoming either. The electron–electron interaction is stronger at lower densities and the system transcends the scope of the Fermi liquid model. The model that describes the behaviour of such a low-density, highly correlated, 1D electron liquid is the TL model, as was also pointed out in the introduction. The fabrication of a 1D semiconducting QW of such low densities is within the reach of state-of-the-art technology. Hence experimental investigations in this regard will determine how far calculations based on the SPA represent the experimental results.

4. Conclusions

We calculated the paramagnon frequency, the magnetic structure factor, and the parallel and anti-parallel spin pair correlation functions using the improved RPA that incorporates the LFC within the HA. The numerical results obtained in the SPA are in very close quantitative agreement with that of the full HA for low-electron-density quantum wires (density $\leqslant 10^6$). An analytical result obtained for the magnetic structure factor also reproduces a similar result for small momentum transfers which depend on the values of electron density considered. The formalism complies with the conservation laws and sum-rules. Numerical results displayed are

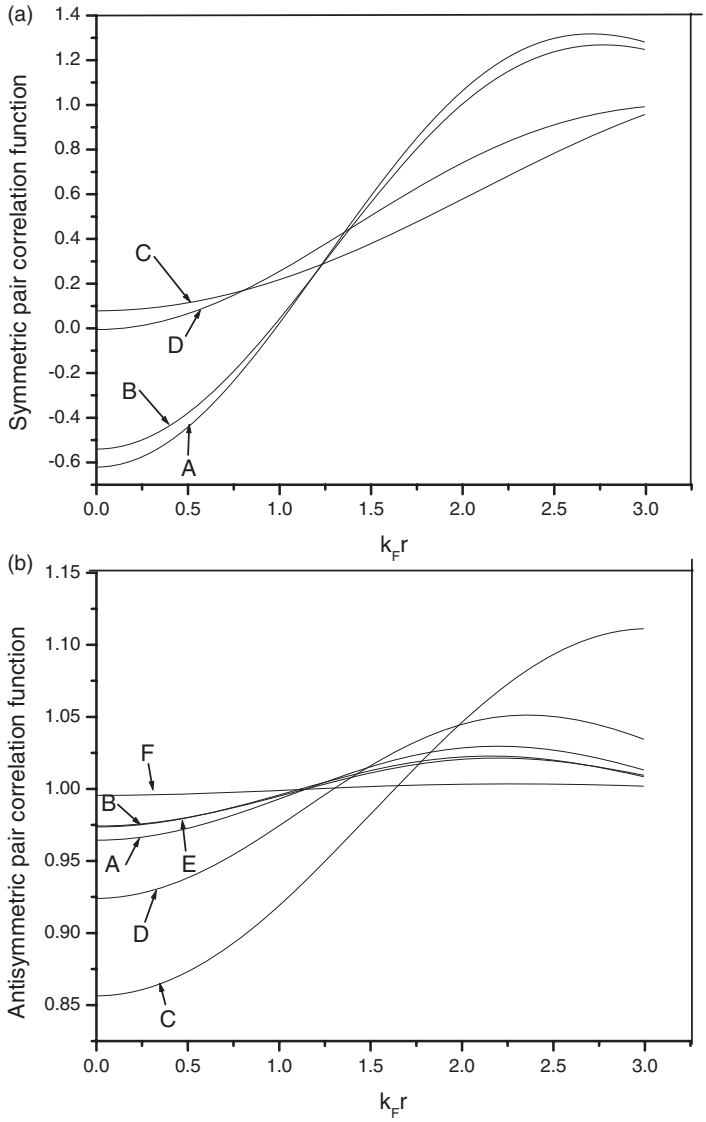

Figure 4. (a) Symmetric spin pair correlation function, $g\uparrow\uparrow(r)$, is plotted as a function of $k_F r$. Figure depicts curves for $g\uparrow\uparrow(r)$ using the SPA $\hat{S}(z)$ (curves A and C) and solving $\hat{S}(z)$ from equation (2) (curves B and D) for two values of $r_s = 1$ and 0.323, respectively, at $a = 7$ nm. (b) Anti-symmetric pair correlation function, $g\uparrow\downarrow(r)$, as a function of $k_F r$. Figure depicts curves (A, C and D) for $g\uparrow\downarrow(r)$ with the use of the SPA $\hat{S}(z)$ and curves (B, D and E) with use of $\hat{S}(z)$ from equation (2). The curves A, B, C, D, E and F are plotted for the following parameters, respectively: curves A and B, $r_s = 1$ at $a = 7$ nm; curves C and D, $r_s = 0.323$ at $a = 7$ nm; curves E and F, $r_s = 1$ at $a = 5$ nm.

those for a GaAs-QW. The results have been found to be in good qualitative agreement with the previously reported self-consistent field calculations of SSTL and STLS. It is envisaged that an experimental investigation in this direction will truly be rewarding and also will ratify the validity of the approach.

Acknowledgments

The authors acknowledge with thanks financial support from the Department of Science and Technology, Ministry of Science and Technology, New Delhi, through a research project.

References

[1] Bulutay C and Tanatar B 2002 *Phys. Rev.* B **65** 195116 and references therein
[2] Reilly D J, Buehler T M, O'Brien J L, Hamilton A R, Dzurak A S, Clark R G, Kane B E, Pfeiffer L N and West K W 2002 *Phys. Rev. Lett.* **89** 246801
[3] Shashkin A A, Anissimova S, Sakr M R, Kravchenko S V, Dolgopolov V T and Klapwijk T M 2006 *Phys. Rev. Lett.* **96** 036403
[4] Ball P 2000 *Nature* **404** 918
[5] Tao N J 2006 *Nat. Nanotechnol.* **I** 173
[6] Luttinger J M 1963 *J. Math. Phys.* **4** 1154
Tomonaga S 1950 *Prog. Theor. Phys.* **5** 644
[7] Hu B Y-K and Das Sarma S 1993 *Phys. Rev.* B **48** 5469
Hu B Y-K and Das Sarma S 1992 *Phys. Rev. Lett.* **68** 1750
[8] Thomas K J *et al* 1996 *Phys. Rev. Lett.* **77** 135
[9] Green F, Neilson D, Swierkowski L, Szymanski J and Geldart D J W 1993 *Phys. Rev.* B **47** 4187
[10] Gold A 1997 *Phys. Rev.* B **55** 9470
[11] Calmels L and Gold A 1997 *Europhys. Lett.* **39** 539
[12] Tanatar B 1996 *Physica* B **228** 329
[13] Tas M and Tomak M 2004 *Phys. Rev.* B **70** 235305
[14] Lobo R, Singwi K S and Tosi M P 1969 *Phys. Rev.* **186** 470
[15] Nagao T, Yaginuma S, Inaoka T and Sakurai T 2006 *Phys. Rev. Lett.* **97** 116802
[16] Caula M, Sorella S and Senatore G 2006 *Phys. Rev.* B **74** 245427 and references therein
[17] Zhao X, Wei C M, Yang L and Chou M Y 2004 *Phys. Rev. Lett.* **92** 236805
[18] Rurali R 2005 *Phys. Rev.* B **71** 205405
[19] Lu Z H, Lockwood D J and Baribeau J-M 1995 *Nature* **378** 258
[20] Van Buuren T, Dinh L N, Chase L L, Siekhaus W J and Terminello L J 1998 *Phys. Rev. Lett.* **80** 3803
[21] Himpsel F J, Kirakosian A, Crain J N, Lin J L and Petrovykh D Y 2001 *Solid State Commun.* **117** 149
[22] Das Sarma S, Hwang E H and Zheng L 1996 *Phys. Rev.* B **54** 8057 and references therein
[23] Ashraf S S Z and Sharma A C 2005 *J. Phys.: Condens. Matter* **17** 3043–59
[24] Mahan G D 1990 *Many Particle Physics* 2nd edn (New York: Plenum)
[25] Li Q P and Das Sarma S 1991 *Phys. Rev.* B **43** 11768
[26] Senatore G and March N H 1994 *Rev. Mod. Phys.* **66** 445
[27] Vashista P and Singwi K S 1972 *Phys. Rev.* B **6** 875
[28] Semiromi E and Ebrahimi F 2006 *Phys. Rev.* B **73** 195418
[29] Li Q P, Das Sarma S and Joynt R 1992 *Phys. Rev.* B **45** 13713